The deep Earth origin of the Iceland plume and its effects on regional surface uplift and subsidence

N. Barnett-Moore[1], R. Hassan[1], N. Flament[1,2], R. D. Müller[1]

* Correspondence to: nicholas.barnett-moore@sydney.edu.au

5 [1]*Earthbyte Group, School of Geosciences, The University of Sydney, NSW 2006, Australia, Email:*
nicholas.barnett-moore@sydney.edu.au

[2]*Now at School of Earth and Environmental Sciences, University of Wollongong, Northfields Avenue,*
Wollongong, NSW 2522, Australia

10 **Abstract.** The present-day seismic structure of the mantle under the North Atlantic indicates that the Iceland hotspot represents the surface expression of a deep mantle plume, which is thought to have erupted in the North Atlantic during the Paleocene. The spatial and temporal evolution of the plume since its eruption is still highly debated, and little is known about its deep mantle history. Here, a paleogeographically constrained global mantle flow model is used to investigate the evolution of deep

15 Earth flow and surface dynamic topography in the North Atlantic since the Jurassic. The model shows that over the last ~ 100 Myr a remarkably stable pattern of convergent flow has prevailed in the lowermost mantle near the tip of the African Large Low-Shear Velocity Province (LLSVP), making it an ideal plume nucleation site. The present-day location of the model plume is ~ 10° southeast from the inferred present-day location of the Iceland plume. We apply a constant surface rotation to the model

20 through time, derived from correcting for this offset at present-day. A comparison between the rotated model dynamic topography evolution and available offshore geological and geophysical observations across the region confirms that a widespread episode of Paleocene transient uplift followed by early Eocene anomalous subsidence can be explained by the mantle-driven effects of a plume head ~ 2000 km in diameter, arriving beneath central western Greenland during the Paleocene. The rotated model

25 plume eruption location beneath Western Greenland is compatible with previous models. The mantle flow model underestimates the magnitude of observed anomalous subsidence during the Paleocene in some parts of the North Atlantic by as much as several hundred meters, which we attribute to upper mantle convection processes, not captured by the model.

30 **Keywords:** Iceland, plume, mantle convection, uplift, subsidence

1. Introduction

The Iceland hotspot is widely recognised as the surface expression of a deep mantle plume, originating from the core-mantle boundary (Morgan, 1971), erupting in the North Atlantic during the Paleocene (Saunders et al., 1997; White and McKenzie, 1989). Its evolution is thought to have significantly

35 influenced the complex continental breakup history of the North East Atlantic (Skogseid et al., 2000), and the V-shaped ridges of thick oceanic crust that characterise the unique seafloor spreading regime of

the region (Parnell-Turner et al., 2014; Smallwood and White, 2002; White et al., 1995). Offshore, numerous efforts have focused on investigating the spatial and transient evolution of the plume since its eruption using tectonic subsidence analysis in Mesozoic basins across the region, which identify either (1) an absence of thermal subsidence during the Paleocene (Clift and Turner, 1995, 1998), (2) an anomalous increase in subsidence during the Eocene (Stoker, 1997; Joy, 1992), or (3) preserved Paleocene transient uplift (Fletcher et al., 2013; Clift and Turner, 1998). Previous seismic studies support these findings, interpreting Paleocene unconformities buried by deep-water sediment during the Eocene, reflecting the transient effects of a mantle plume (Champion et al., 2008; Smallwood and Gill, 2002; Clift, 1996). Onshore, fission track studies that constrain denudation histories (Green, 2002; Lewis et al., 1992) suggest that exhumation across northern England can be explained by topographic doming over a mantle hotspot (Lewis et al., 1992). Extrusive volcanics peppered across isolated parts of the North East Atlantic have also been dated and linked to the arrival and relative motion of the Iceland plume beneath the region (Tegner et al., 2008; Storey et al., 2007; Saunders et al., 1998; Upton et al., 1995; Noble et al., 1988). The motion path of the Iceland plume is elusive as large ice sheets over Greenland currently mask geological evidence that could potentially resolve this debate (Rogozhina et al., 2016). End-member plume motion paths have been proposed (see Rogozhina et al., 2016 for a discussion) based on a moving hotspot reference frame constrained by the hotspots in the Indo-Atlantic oceans (O'Neill et al., 2005) or, alternatively, constrained by hotspots in the Indo-Atlantic and Pacific oceans (Doubrovine et al., 2012). Nevertheless, the understanding of the time-dependent evolution of the deep Earth convective engine beneath the region before 60 Ma remains limited. The latest studies on deep Earth dynamics argue that over the last 300 Myr a majority of plumes originated at the edges of two pronounced LLSVPs beneath Africa and the Pacific Ocean (Doubrovine et al., 2016). Previous mantle flow models show that the morphology of the LLSVPs is modulated by subduction-induced flow in the lowermost mantle (Bower et al., 2013, Hassan et al., 2015; 2016). These results indicate that considering the time-dependent evolution of the lower mantle beneath the North Atlantic and the contributions of subduction-induced flow in the vicinity may shed some light on the spatial and the temporal evolution of the Iceland plume.

Here, we numerically simulate the evolution of the Iceland plume by using a paleogeographically constrained geodynamic model (e.g. Hassan et al., 2015; 2016). We compare the model dynamic topography evolution to available geological and geophysical observations in the region, including published tectonic subsidence curves (Jones et al., 2001; Clift and Turner, 1998; Clift et al., 1998), analytically modelled transient uplift histories (Hartley et al., 2011; Champion et al., 2008), stratigraphically modelled uplift histories (Nadin et al., 1995), and published locations of plume-related extrusive volcanics (as compiled in Torsvik et al. 2001 and updated in Torsvik et al. 2015) in order to understand the mantle-driven effects of the near-surface arrival of the Iceland plume on the evolution of surface topography in the North Atlantic. We also compute the motion path of the model plume through time and compare it to other published end-member motion paths. To understand the deep mantle source of the Iceland plume beneath the North Atlantic, we analyse the mean flow patterns in a 300 km thick shell above the core-mantle boundary (CMB) and evaluate the stability of the northernmost edges of the African LLSVP over time.

2. Methods

2.1 Numerical models of mantle convection

We devise numerical models of convection within the Earth's mantle under the extended-Boussinesq approximation (Christensen and Yuen, 1985). The Earth's mantle is modelled as a spherical shell with depth-dependent thermodynamic properties and temperature- and depth-dependent rheology, where the deepest lower mantle is chemically heterogeneous. We solve the equations for the conservation of mass, momentum and energy using the parallel finite element code CitcomS (Zhong et al., 2008), which has been extended to allow for assimilation of surface plate motion and subducting slabs derived based on global plate reconstructions (Bower et al., 2015).

The underlying assumptions and our choice of model parameters employed have been outlined in earlier work (Hassan et al., 2015; Bower et al., 2015). Table 1 lists important model parameters and additional details can be found in Hassan et al. (2015).

2.1.1 Model setup

The spherical mesh representing the Earth's mantle comprises ≈12.6 million mesh elements, where radial mesh refinement provides a vertical resolution of ≈15 km and ≈27 km near the top and bottom boundary layers, respectively. The temperature decreases by 1225 K in both the top and the bottom thermal boundary layers. Away from the thermal boundary layers, we assume an a priori mantle adiabat with a potential temperature of 1525 K. In all model cases we specify a non-dimensional internal heat generation rate of 100 and a reference profile for thermal expansion based on analytical parameterizations given in Tosi et al. (2013).

We use piecewise Arrhenius laws to describe the variation of viscosity with temperature, depth and composition in the Earth's mantle, which takes the following non-dimensional form:

$$\eta(T, r) = A(r)\eta_c \exp\left(\frac{E_a(r) + (1-r)V_a(r)}{T + T_{off}} - \frac{E_a(r) + (1 - r_{inner})V_a(r)}{1 + T_{off}}\right), \quad (1)$$

where η is the viscosity, T is the temperature, r is the radius, A is the pre-exponential parameter, η_c is the intrinsic composition-dependent pre-factor, E_a is the activation energy, V_a is the activation volume and T_{off} is the temperature offset. For the lower mantle, we use a dimensional activation energy of 320 KJ mol^{-1} and activation volume of 6.7E-6 m^3 mol^{-1}, corresponding to non-dimensional units of 11 and 26, respectively, which are comparable to estimates in Karato and Wu (1993). However, since such viscosity parameterizations lead to large viscosity variations that cause numerical difficulties, we adjust the pre-exponential parameter A(r) and the temperature offset T_{off} (Tackley, 1996) to limit the viscosity contrast to 3 orders of magnitude. The resulting viscosity profile is similar to the preferred viscosity profiles of Steinberger and Calderwood (2006). Additional details on model setup can be found in Hassan et al. (2015).

The initial condition at 230 Ma includes slabs inserted from the surface down to 1200 km depth, and an anomalously dense thermochemical layer of uniform thickness at the base of the mantle. We apply kinematic surface boundary conditions based on surface velocities derived from global plate tectonic reconstructions at one million year intervals, with a linear interpolation in between. We assimilate

5   thermal models of inferred subducting slabs into the dynamically evolving temperature field at each timestep, as the model progresses towards present-day, starting from a given geological time (see Bower et al., (2015), for more detail).

2.1.2 Computation of Dynamic Topography

10   We compute time-dependent dynamic topography, h, at the surface at 5 Myr intervals as:

$$h = \frac{\sigma_{rr}}{\Delta \rho g} \qquad (2)$$

where σ_{rr} and $\Delta \rho$ are the radial component of stress and the density difference between the mantle and the overlying material, respectively. The radial stresses, σ_{rr}, are recomputed using Stokes flow and the temperature field at a given time. We exclude buoyancy in the top 350 km of the mantle in the Stokes flow computations in order to remove the influence of assimilated data. Moreover, to exclude the

15   traction induced by kinematic plate velocities (velocity boundary condition at the surface), we impose free-slip boundary conditions at the surface in these Stokes flow computations.

2.2.3 Parameter space explored

20   We interrogate the models described in Hassan et al. (2015), where the density contrast ($\Delta \rho_{ch}$) of a dense chemical layer above the CMB and the thickness of the dense layer (Δd) was varied, keeping all other parameters constant. The first model plumes to erupt in models with a dense layer above the CMB erupt between 185 Ma and 119 Ma – a clear trend is observed, where increasing density contrasts and thicknesses of the dense layer lead to a delayed nucleation of plumes. While Hassan et al. (2015)

25   derived spatial correlations of distributions of model plume eruption locations with reconstructed eruption locations of Large Igneous Provinces (LIPs), their study did not account for temporal misfits between model plumes at robust plume nucleation sites and related LIPs – e.g. the model Iceland plume in their preferred case M5 erupts at 150 Ma. The temporal misfits are partly a consequence of model initiation times and idealized initial conditions adopted due to a lack of constraints on the

30   structure of the mantle in deep geological time and more generally due to the stochastic nature of plume dynamics.

Devising forward mantle convection models that reproduce model plume eruptions that match associated LIP eruptions in both space and time would require an elaborate iterative optimization scheme. The distribution of thermal and compositional heterogeneities in the deep lower mantle would

35   be iteratively constrained in a bid to reduce space-time misfits between model plume eruptions and associated LIPs, which is beyond the scope of this study. Here we extend the parameter space explored in Hassan et al. (2015) to include model initiation times. We take their preferred model, case M5, and

systematically vary the model initiation time to obtain a model in which the Iceland plume arrives near the surface at ~ 60 Ma. We find that with a model initiation time of 140 Ma, the near-surface (350 km depth) arrival of the Iceland plume is consistent with the timing of the onset of magmatism associated with the Iceland plume at ~ 60 Ma in the north Atlantic (Torsvik et al., 2001). This model constitutes

5 the basis for all analyses presented in this study.

The first order, present-day structure of the mantle in our preferred model is similar to that in case M5 in Hassan et al. (2015); the deep lower mantle is dominated by a degree 2 structure of anomalously dense material, representing the two LLSVPs. Although, the case presented here features fewer plumes at present compared to that in M5 (Hassan et al., 2015), and significant temporal misfits are observed

10 between other model plumes and associated LIPs. This is an expected outcome, however, since the model is tuned to produce a model Iceland plume that temporally matches associated geological observations.

3. Deep Earth origin of the Iceland plume and associated dynamic topography evolution

3.1. Predicted spatio-temporal evolution of the deep mantle flow beneath the North Atlantic

15 Analysing lowermost mantle flow under the north Atlantic reveals a consistent pattern of convergent flow over the last 100 Ma near the tip of the present-day African LLSVP. Time-averaged flow directions and contours of the mean location of the model LLSVP (Fig. 1) over the period suggest that a stable plume nucleation site has prevailed in the North Atlantic, near the present-day Iceland plume, well before its nucleation. Southeasterly flow from the west and northwesterly flow from the east

20 converge in a lowermost mantle stagnation zone under the British Isles, in which the time-averaged flow is close to zero (Fig. 1). Moreover, the mean location of the northern extremity of the model African LLSVP (solid red contours, Fig. 1) over the last 100 Ma is in reasonable agreement the present-day tomography (yellow contour in Fig. 1), albeit shifted to the southeast.

25 #### 3.2 Applying a global surface rotation to our preferred dynamic topography model through time

The present-day model Iceland plume is ~10° southeast of the present-day location of the Iceland plume (Fig. 1) inferred by Torsvik et al. (2015; *see their Fig. 1*; black arrow in Fig. 1). Here, we consider a scenario in which the surface location of our model plume evolves through time, such that it ends up at its observed present-day location (as in Torsvik et al., 2015; Fig. 2). From this we can

30 compare the predicted dynamic topography evolution to a compiled set of observables preserving evidence of anomalous vertical motions in the region (Figs 4-9), and assess the reconstructed model motion path of the Iceland plume since the Paleocene against previously published motion paths (e.g. Torsvik et al., 2015; Doubrovine et al., 20102; O'Neill et al., 2005). To do this, we apply a finite rotation using the GMT program grdrotater (Wessel et al., 2013) to the model results, using the

35 proposed present-day location of the Iceland plume to define a fixed Euler pole. We apply the same surface rotation using this fixed Euler pole back to 70 Ma, as a mantle plume at the surface is not

predicted for earlier times (Fig. 3). The rotation of the model results, illustrated by the black arrow in Fig. 3J, re-locates the distribution of dynamic topography magnitudes and its spatial evolution through time (Fig. 3).

The rotated results imply near-surface arrival (~ 60 Ma) of the model Iceland plume somewhere

5   beneath Disko Island, along the central western Greenland margin (Fig. 3). The Iceland plume then migrates eastward across the continent, arriving at the present-day coastline of the east Greenland margin by ~ 35 Ma. Following this, it begins its southeastward decent towards the present-day location of its conduit (Fig. 3). The predicted motion of the rotated model plume is compatible with the spatial and temporal evolution of plume-related magmatism within the North Atlantic (Fig. 3C-H). The

10   evolution of dynamic topography magnitudes through time shows maximum dynamic uplift is spatially largest at ~ 60 Ma, ~ 2000 km in diameter. This is focused beneath central Western Greenland, and extends across the entire North Atlantic (Fig. 3C). At this time the effect of the dynamic uplift related to the near surface arrival of the model plume encompasses parts of the Artic to the north, beyond Baffin Bay in the North American continent to the west, the Labrador Sea and Orphan Basin to the

15   south, and the Norwegian margins and Mesozoic Basins lining the northwest European margin to the east (Fig. 3C). Post ~ 60 Ma, the model plume greatly diminishes in spatial extent by more than half to ~ 1000 km in diameter, resulting in dynamic subsidence of these surrounding regions until ~ 40 Ma (Fig. 3D-3F). By this time, the plume has migrated eastward and straddles the Norwegian margin and Mesozoic basins along the northwest European margins (Fig. 3G-3J) of the early northeast Atlantic

20   Ocean. This results in a reversal from dynamic subsidence to dynamic uplift across these major basins, a phenomenon that continues until present-day as the plume migrates further eastward (Fig. 3G-3J).

4. Comparing the predicted Iceland plume motion and associated topography to geological and geophysical observations

25   To evaluate the evolution of rotated dynamic topography through time (section 3.2) we assess (1) the absolute and relative motion path of the model Iceland plume in the context of previously published plume motion paths (section 4.1), (2) the timing and location of its near surface arrival (section 4.1, 4.2), and (3) its contributions to the regions topographic vertical motions through time via a comparison with tectonic subsidence histories and other related studies (section 4.2).

30   **4.1 Comparing the rotated plume motion path against previous Iceland plume motion paths**

We compare the absolute motion path of our model plume to previous efforts (Fig. 2) that have derived its motion path through generating new global absolute plate reference frames (e.g. Doubrovine et al., 2012 and O'Neill et al., 2005). We extract the absolute motion path of the Iceland model plume based on a plume detection scheme (described in detail in Hassan et al., 2015) that detects all model plumes

35   at a given time instance. The spatial locations of model plumes, throughout the modelled geological time, are then binned together based on spatio-temporal proximity to derive absolute motion paths of respective model plumes (for more details see Hassan et al., 2016). We also compute the motion path

of the Iceland plume relative to Greenland using GPlates (Boyden et al., 2011), for comparison in this frame of reference (e.g. Rogozhina et al., 2016).

Doubrovine et al. (2012) proposed a global moving hot spot reference frame from backward advected numerical convection models. This method is constrained by a number of well-studied hot spot tracks

5 in the Indo-Atlantic and Pacific, and global plate reconstructions (Doubrovine et al., 2012). This reference frame challenges the validity of traditional absolute reference frames that assume hot spots are fixed through time (Muller et al., 1993; Morgan, 1971). O'Neill et al. (2005) used Indo-Atlantic hot spot tracks to produce both a fixed and moving hot spot reference frame, and found that the two were nearly indistinguishable over the last ~ 80 Myr, concluding that any hot spot motion within the mantle

10 was not obvious beyond the uncertainties in the data (O'Neill et al., 2005). A key difference between the approach of Doubrovine et al. (2012) and O'Neill et al. (2005) is the number of hotspots used in each study (Torsvik et al., 2015). O'Neill et al. (2005) only considered the Indo-Atlantic hotspots, whereas Doubrovine et al. (2012) included hotspots from the Indo-Atlantic and Pacific. Tracking past motions of the Iceland plume remains elusive (O'Neill et al., 2005; Doubrovine et al., 2012; Torsvik et

15 al., 2015; Rogozhina et al. 2016) because thick ice sheets currently cover any potentially preserved geological evidence of its path beneath Greenland. Therefore, the motion path of the Iceland plume is inferred in any reference frame, based on the fit of other hot spot tracks in either the Indo-Atlantic, or Indo-Atlantic and Pacific, combined with the relative plate circuits chosen for the North Atlantic.

20 A comparison between the absolute motion path (AMP) of our model plume and Doubrovine et al. (2012) shows good agreement until ~ 30 Ma, at which time the paths significantly deviate (Fig. 2). For the last ~ 30 Myr the match between our model and Doubrovine et al. (2012) seems reasonable. However, limitations of backward advection modelling introduce uncertainty into the reference frame of Doubrovine et al. (2012). The time interval over which backward advection models can reliably

25 reproduce past mantle structures is fundamentally limited (Ismail-Zadeh et al., 2009). This time interval is short - relative to the lifespan of a mantle plume - for conduction-dominated heat transfer, such as during the conductive thickening of the lower thermal boundary layer associated with plume nucleation. In addition the approach in e.g. Doubrovine et al. (2012) and O'Neill et al. (2005) does not consider the evolution of mantle plumes in a self-consistent numerical flow field, instead tracking the

30 advection by mantle flow of particles seeded at plume locations. The relative moving and fixed motion paths (RMP) of our model plume beneath Greenland differs from both that of Doubrovine et al. (2012) and that of O'Neill et al. (2005) (Fig. 2A). In the model of Doubrovine et al. (2012) the Iceland plume is located beneath East Greenland before ~ 35 Ma (Fig. 2). Torsvik et al. (2015) state that this is a remarkably good fit given the long-term volcanic activity in the immediate vicinity the plume between

35 30-60 Ma (Fig. 3). They also note that unusually thin lithosphere in the region (< 100 km; Rickers et al., 2013) provides further evidence of longstanding plume-lithosphere interactions, as they attribute this thinning to thermal and mechanical erosion (Steinberger et al., 2014) due to the plume head (Torsvik et al., 2015). However, this inferred location of the Iceland plume at 60 Ma is difficult to reconcile with the contemporaneous eruption of extrusive volcanics attributed to the arrival of the

40 Iceland plume along the West Greenland margin, and on Baffin Island also (Spice et al., 2016; Stuart et

al., 2003; Chalmers et al., 1995). Previous compilations of fission track data and dated extrusive magmatism across the northeast Atlantic (Clift et al., 1998; *see their Fig. 9*), or onshore geology and offshore seismic interpretations (Skogseid et al., 2000) also suggest the plume centre was located beneath central western Greenland during the Paleocene. In addition, the reference frame of Doubrovine et al. (2012) implies an unusual motion path of the plume beneath Greenland between ~ 65 and 50 Ma (Fig. 2B). From 60-65 Ma the implied plume motion is eastward, abruptly changing to short-lived westward motion until 55 Ma when it again abruptly changes to a more southward motion until present-day (Fig. 2B).

Comparing the relative motion path (RMP) of our model plume beneath Greenland to that of O'Neill et al. (2005) shows a better general agreement over the last 60 Myr, although the relative motion path of our model plume is further south prior to ~ 20 Ma (Fig. 2). Rogozhina et al. (2016) used ice-penetrating radar and ice core drilling to identify melting beneath the Greenland Ice Sheet, which they attribute to a large geothermal anomaly beneath Greenland and associate with the Iceland plume track between ~ 80-35 Myr ago (Fig. 2A). The moving hot spot path of O'Neill et al. (2005), which is the northernmost of the currently proposed end-member motion paths, best fits that proposed Iceland plume motion path (Rogozhina et al., 2016).

A thermal anomaly can be traced continuously westward beneath Baffin Bay and the Davis Straight (Jakovlev et al., 2012), a region that reflects a now extinct seafloor spreading system (Fig. 2A; Oakey and Chalmers, 2012). This outlines the difficulty involved in defining the true extent of this thermal anomaly, reflecting the Iceland plume motion path, as its western extent merges into a recently thinned and heated continental margin region (Fig. 2A). A recent high-resolution S-velocity model of the North Atlantic region, *"revealing structural features in unprecedented detail down to a depth of 1300 km"* (Rickers et al., 2013), does not appear to identify any shallow thermal anomaly beneath this region of Greenland. Other regional geological observations indicate that a thick cratonic root exists within southern Greenland (Fig. 2A; Artemieva, 2006), which may have played a significant role in plume-lithosphere interactions during the early Cenozoic. We suggest that the motion path of our model plume would have straddled this craton during the early Cenozoic, resulting in less obvious mechanical and thermal erosion of this much thicker lithosphere in the first ~ 10-15 Myr of plume motion (Fig. 2A). The existence of this craton also suggests that the thin thermal anomaly identified by Rogozhina et al. (2016) could represent differences in the geological structures across Greenland rather than the remnants of a plume track. The work of Kaban et al. (2014), who used a numerical approach to decouple the effects of lithospheric plates and the observed geoid globally at present-day, indicates that at present-day ~ 500 m dynamic support across central Greenland is confined to the extent of a 'thin finger' traversing from the present-day Iceland plume conduit to Disko Island along the central western Greenland (Kaban et al., 2014; *see their Fig. 8A*). This dynamic support mirrors our predicted plume motion. Fahnestock et al. (2001) used ice-penetrating radar to reveal that localised regions in southern Greenland undergoing rapid basal melting at present-day coinciding with magmatic anomalies and topography associated with volcanic activity (Fahnestock et al., 2001). The extent and magnitude of this basal melt in southern Greenland is in close vicinity of the early motion path of the model plume

(Fahnestock et al., 2001; *see their Fig. 1*). This volcanic activity could be linked to remanent plume activity along the Iceland plume motion path.

4.2 Comparing predicted dynamic topography to a compiled set of observables on anomalous uplift and subsidence in the North East Atlantic

4.2.1 Identifying post-rift anomalous subsidence

The stretched continental margins of the North Atlantic region reflect major episodes of extension since the Late Paleozoic, which have contributed to the evolution of regional surface topography (Skogseid et al., 2000). The spatial and temporal progression of this continental extension can be understood in terms of evolving patterns of subsidence that reflect rates of crustal thinning and changes in lithospheric heat flow (Jarvis and McKenzie, 1980). During extension the lithosphere thins rapidly, producing rapid subsidence and an accompanying thermal positive anomaly (Jarvis and McKenzie, 1980). Upon cessation of this extension the thermal anomaly begins to decay due to thermal re-equilibration, resulting subsidence rates slowing according to a half-space cooling model (Jarvis and McKenzie, 1980). As the vast majority of data compiled in this study is located in major basins across the northeast Atlantic (Fig. 4) we used inferred extensional histories of these basins to derive theoretical water-loaded tectonic subsidence histories, identifying any significant deviations from these as anomalous subsidence (Erratt et al., 1999). We compiled data from sites in the Porcupine, Rockall, Faroe-Shetland, North Sea, and southern Møre Basins, as well as two locations along the east and west Greenland margins (Fig. 4). As an example of identifying anomalous subsidence we compare water-loaded tectonic subsidence derived from a backstripped well in the North Sea (Fig. 5A; Clift and Turner, 1998) to an expected equivalent water-loaded tectonic subsidence history modelled using a time-dependent analytical approach assuming different stretching factors (Fig. 5A; Jarvis and McKenzie, 1980). Well 13-27-1 (Clift and Turner, 1998) shows a syn-rift stage of subsidence that occurred between 135 and 160 Ma (Fig. 5A). In the absence of control points after this time period we assume a change to post-rift at 135 Ma (Fig. 5A). During the initial post-rift stages subsidence rates decline until ~ 100 Ma where an onset in gentle uplift is recorded until ~ 65 Ma. By this time rapid transient uplift occurs (Clift and Turner, 1998), peaking at ~ 62 Ma and declining by 60 Ma, remaining relatively unchanged until present-day. In comparison, theoretical tectonic subsidence histories for well 13-27-1 (Fig. 5B, Fig. 6B) predict very low post-rift subsidence, declining in magnitude throughout the Cenozoic, and continuing like-so until present-day. The mismatch between predicted and inferred subsidence for this well, with ~400-600 m less subsidence than predicted at 60 Ma and ~ 150-350 m less subsidence than expected at present day and (Fig. 5), is attributed to the influence of the Iceland plume that is not included in the tectonic subsidence model. Where published well locations have a reasonably good constraint on synrift and post-rift stages of a basin, we compute anomalous vertical motion curves that show the differences between the backstripped tectonic subsidence history and forward modelled tectonic subsidence history (Figs 5B, 6M-6R, 7I-7L, 8I-8L). We compute an ideal stretching factor that either best matches the onset in the syn-rift, or post-rift stage, which is then used to calculate the inferred tectonic subsidence history. Differences taken between the two curves represent anomalous vertical motions through time unrelated to thermal cooling of the lithosphere

during the post rift stages (Fig. 5B, 6M-6R, 7I-7L, 8I-8L). In wells appropriate for this calculation across the NE Atlantic we focus on anomalous vertical motions for the last 70 Myr only, in accordance with the temporal extent of our rotated dynamic topography model (section 3.2). When using this approach to identify anomalous vertical motions we note that (1) we expect to observe a slow decay in

5   low post-rift subsidence rates during the Cenozoic if extension in a given basin ceased some time during the Cretaceous, (2) we can investigate the spatial and temporal links between modelled anomalous vertical motion curves and the arrival of the Iceland plume (section 3), (3) we can make spatial inferences about the extent of the Iceland plume from the anomalous vertical motions calculated where possible, and (4) we can compare the timing and magnitude of anomalous vertical motion curves

10   with the predicted rotated dynamic topography since the Paleocene.

4.2.2 Anomalous vertical motions from wells in the North Sea basins

In the North Sea published backstripped wells include control points that cover the pre-rift, synrift, and post-rift stages of basin evolution (Fig. 6; Clift and Turner, 1998). Generally, subsidence histories in the region indicate a major phase of extension lasting between ~160-135 Ma (Fig. 6A-F). Following

15   this, each well records a history of post-rift subsidence that is at odds with the theoretical tectonic subsidence curve (Fig. 6; section 4.2.1). As the basins in the North Sea did not experience any secondary extensional episodes after the late Jurassic (Erratt et al., 1999) we assess the compatibility of the rotated model dynamic topography (section 3.2) with this Cenozoic anomalous subsidence.

In these wells inferred anomalous subsidence during the Paleocene may be recorded either as (1)

20   transient uplift between ~ 65-62 Ma (13-27-1; Fig. 6B, 6H) if enough control points are available, (2) permanent uplift (11-25-1; Fig. 6A, 6G, 12-21-5; Fig. 6F, 6L), or (3) anomalous accelerated subsidence from ~ 60 Ma (14-19-9; Fig. 6C, 6I, 21-2-1; Fig. 6D, 6J, 15-17-9; Fig. 6E, 6K). We compare the predicted evolution of rotated dynamic topography for each of these well locations back to 70 Ma to their respective subsidence curves, both of which have been set to zero elevation at present-day (Fig.

25   6G-L). Generally, dynamic topography evolves similarly across all well locations, which is to be expected given its spatially long wavelength (e.g. Flament et al., 2013). In this region, the model predicts ~ 250 m of dynamic uplift from 70-60 Ma, then ~ 100 m of dynamic subsidence until 55 Ma, which plateaus until 50 Ma before renewed dynamic subsidence by ~ 300 m between ~50-33 Ma. Following this, ~250 m of dynamic uplift occurs until ~ 20 Ma by which age dynamic topography is

30   essentially constant until present-day. The model dynamic topography fits the timing and amplitude of anomalous subsidence during the late Paleocene and early Eocene for wells 14-9-9 and 15-17-9 (Fig 6I, 6K). Dynamic topography agrees temporally with the cessation in uplift by ~ 60 Ma for wells 11-25-1, 13-27-1 and 12-21-5 (Fig. 6G, 6H, 6L), and with the onset in rapid anomalous subsidence from ~ 60 Ma for well 21-2-1 (Fig. 6J). Well 13-27-1 (Fig. 6H) indicates transient dynamic uplift at ~ 60Ma,

35   which is temporally offset from our model results by only ~ 3 Myr (section 4.2.1). The temporal evolution of dynamic topography magnitudes agree reasonably well with the magnitude of anomalous transient uplift highlighted by anomalous vertical motions (Fig. 6M-6R) where permanent uplift, associated with underplating, is not observed e.g. well 11-25-1 and well 12-21-5 (Fig. 6M, 6R). Maximum dynamic uplift falls within the error range of the anomalous transient uplift, associated with

40   the inherited uncertainty of palaeobathymetry depths at those ages (Fig. 6M-6R).

Bertram and Milton (1989) derived a basin history at a well in the North Viking Graben (Fig. 9G). This water-loaded tectonic subsidence curve is tied to sea level at four points (published without palaeobathymetry error bars) and assumes two rifting episodes in the Triassic and Jurassic with

5   stretching factor of 1.35, and ~ 300 m of modelled anomalous Paleocene uplift (Fig. 9G; Bertram and Milton, 1989). This subsidence history agrees well with those of Clift and Turner (1998) (Fig. 6) lending support to the regional-scale extent of anomalous Paleocene subsidence across the North Sea. A comparison between the tectonic subsidence history derived in Bertram and Milton (1989) and our dynamic topography (Fig. 9G) shows a temporal offset of ~ 5 Myr in maximum transient uplift, and a

10   ~ 30 m magnitude mismatch. Others who support this Paleocene transient uplift interpret a Paleogene unconformity buried by early Eocene deep-water sediments across the North Sea (Mudge and Jones, 2003; Milton et al., 1990) and pulses of coarse clastic sediment deposited in the northern parts of the North Sea during the earliest Eocene (Huuse, 2002) linked to the Iceland plume. Nadin et al. (1997) used forward and inverse 2-D modelling of syn- and post rift stratigraphy to determine the timing and

15   magnitude of Paleocene uplift associated with the Iceland plume in major basins across this region. For three locations (Fig. 4; pale purple stars) they estimated ~ 375-550 m of anomalous Paleocene uplift and computed its thermal decay through time until present-day (Fig. 9H). Comparing the model dynamic topography extracted at these three points (Fig. 9H) shows (1) agreement in the cessation of dynamic uplift and onset in subsidence at ~ 60 Ma, (2) a mismatch in the magnitudes of total dynamic

20   subsidence since ~ 60 Ma with the model predicting approximately half of what is modelled in Nadin et al. (1997), and (3) a mismatch in vertical motions since ~ 35 Ma (Fig. 9H), as the model predicts an onset in dynamic uplift associated with the eastward migration of the model plume away from Greenland (Fig. 3).

25   In summary, the timing and duration of transient uplift and subsidence predicted by our model are compatible with independent constraints in the North Sea. The amplitude of the predicted uplift is within the palaeobathymetric error of the anomalous vertical motion histories, and underestimates this uplift by ~ 200 m where permanent uplift is recorded. The predicted dynamic uplift from the late Eocene (~ 35 Ma), associated with the eastward migration of the model plume, matches only with well

30   15-17-9, as it is not recorded in the other subsidence histories of the basin (Fig. 6).

4.2.3 Anomalous vertical motions from wells in the Porcupine Basin

In the Porcupine Basin we compile a set of subsidence curves published in Jones et al. (2001) (Fig. 7; Fig. 8). Generally, in this basin post-rift subsidence histories indicate 500-800 m of anomalous transient uplift and subsidence occurred since the Paleocene-Eocene boundary (~ 55 Ma; Fig. 7; Fig. 8;

35   Jones et al., 2001). Similarly to the major basins of the North Sea (section 4.2.2), this basin did not experience any extensional episodes after the early Cretaceous (Tate et al., 1993), suggesting Cenozoic anomalous subsidence recorded in each well across the region is not rift-related. We assess the likelihood that our dynamic topography model (section 3.2) can explain this widespread Paleocene anomalous subsidence. Comparing the predicted dynamic topography against the tectonic subsidence

40   curves of the Porcupine Basin (Fig. 7; Fig. 8) shows a < 10 Myr mismatch in the timing of maximum

dynamic uplift. Temporally, the tectonic subsidence histories commonly show an onset in anomalous transient uplift from ~ 60 Ma, and maximum magnitudes peaking at times between 50 Ma (Fig. 7A, 7E) and 55 Ma (Fig. 7C, 7G). We compute ideal theoretical subsidence histories for each of these wells using the stretching factors and periods published in Jones et al. (2001), and calculate anomalous

5   vertical motion curves as the differences between this inferred subsidence history and the backstripped one (Fig. 7I-7L). Generally, these anomalous vertical motion curves show ~ 400 m of transient uplift followed by ~ 450 m to 700 m (Fig. 8J; Fig. 7J) of anomalous subsidence between 50 and 60 Ma (Fig. 7; Fig. 8). Across the basin, the maximum model dynamic uplift (~ 100 m at ~ 60 Ma) is underpredicted by ~ 500 m, and the subsequent dynamic subsidence is underpredicted by ~ 400-600 m.

10   The dynamic uplift predicted in the model beneath this basin, is weaker here than in the North Sea basins because the Porcupine Basin is on the southeastern edge of the model Iceland plume during the Paleocene (Fig. 3).

This comparison shows the model is compatible with the timing and duration of Paleocene transient

15   uplift and subsidence in the Porcupine Basin, but underestimates the magnitude of that uplift event by several hundred meters. The predicted dynamic uplift from the late Eocene (~ 45 Ma), associated with the large-scale dynamic effects of the eastward migration of the model plume across the northeast Atlantic, is not recorded in the subsidence histories of these basins.

4.2.4 Observations of anomalous vertical motions along the Norwegian margin, and plume-

20   **related transient uplift in the Faroe-Shetland and Møre Basins during the Paleocene**
A structural and stratigraphic analysis along the Norwegian margin in the Vøring Basin, immediately north of the Møre Basin (Fig. 4; Planke et al., 1991), showed that its mode of rifting (Peron-Pinvidic ewt al., 2013) changed from brittle to more ductile extensional deformation during the Paleocene (Ren et al., 2003). This change is related to the arrival of the Iceland plume, and the subsequent initiation of

25   associated igneous activity (Ren et al., 2003). Roberts et al. (2009) mapped eleven horizons from seabed to Base Cretaceous that they backstripped to produce a series of palaeobathymetry and palaeostructure maps across the Møre and Vøring Basins. They incorporated a transient dynamic uplift event of the Norwegian margin during the Paleocene derived from previous estimates made in the Faroe-Shetland Basin (Rudge et al., 2008) as they were unable to distinguish between extension-related

30   and plume-related surface vertical motions within the basins along the Norwegian margin at this time (Roberts et al., 2009; Roberts et al., 1997). Nielsen et al. (2002) analysed the topography, heat flow, crustal structure, and Bouger Gravity of Norway, proposing the region was influenced by surface uplift in the latest Paleocene related to plume emplacement and that its new topography was modulated by changes in climate and eustasy throughout the remaining Cenozoic. Given the current uncertainty in

35   quantifying the magnitude of transient uplift along the Norwegian margin we are unable to directly assess the model dynamic topography for this region. Nevertheless, the consistency of these observations along the Norwegian margin with those compiled around the remainder of the North Atlantic (section 4.2) is compatible with the spatial and temporal extent of the model plume (Fig. 3).

In the Faroe-Shetland and southern Møre Basins (Fig. 4) we compiled a subset of back-stripped water-loaded tectonic subsidence curves from Clift and Turner (1998), which preserve evidence of subsidence histories being 'interrupted' by anomalous transient uplift during, or just before the Paleocene (Fig. 9A-9F). The number of control points used in the construction of these tectonic

5   subsidence curves is generally small for times older than ~ 100 Ma (Fig. 9A-9F). As such we are unable to produce forward models of these subsidence histories with any real confidence given the lack of well constraints compounded by the complexity in the extensional histories of these basins (Skogseid et al., 2000; Brekke et al., 2000). Instead, we make a qualitative comparison between the dynamic model and these subsidence histories, assessing the ability of the model plume to explain the

10   onset and temporal extent of preserved anomalous transient uplift in these basins during the Paleocene. In the Møre Basin, the model predicts ~ 200 m of dynamic uplift from 70 Ma, peaking at 60 Ma, followed by ~ 300 m of gradual dynamic subsidence until ~ 35 Ma and renewed dynamic uplift until the present-day. Well 209-4-1 and 209-9-1 both show maximum transient uplift events occurring during this time at ~ 60 Ma (Fig. 9A), and ~ 55 Ma (Fig. 9B), respectively. This match in the timing of

15   maximum uplift between these wells and the dynamic model illustrates that the model plume can account for this transient uplift event, which interrupts the subsidence histories in the southern Møre Basin. South of this, in the Faroe-Shetland Basin the model predicts ~ 300 m of dynamic uplift from 70 Ma, peaking at 60 Ma, followed by ~ 450 m of rapid dynamic subsidence until ~ 35 Ma and renewed rapid dynamic uplift until ~ 20 Ma, followed by protracted dynamic uplift until the present-

20   day (Fig. 9C-9F). Across the wells in this basin maximum uplift occurs at ~ 55 Ma in well 208-23-1 (Fig. 9C), at ~ 60 Ma in well 205-10-2B (Fig. 9D), at ~ 50 Ma in well 205-22-1 (Fig. 9E), and at ~ 58 Ma in well 164-25-1 (Fig. 9F). A comparison between these four wells and the dynamic uplift predicted from the model shows, again, good agreement on the duration of transient uplift and the timing in peak uplift during the Paleocene. In a related study, Fletcher et al. (2013) used flexural

25   backstripping and decompaction techniques along stratigraphic sections to estimate ~ 450-550 m of Late Paleocene plume-related transient uplift in this basin, suggesting that the dynamic uplift predicted by the model is underestimated by no more than ~ 200 m against this study.

Other studies used three-dimensional seismic reflection data to quantify and temporally constrain the

30   plume-related transient uplift in the Faroe-Shetland Basin (Hartley et al., 2011; Champion et al., 2008; Rudge et al., 2008). Champion et al. (2008) attributed fluvial incisions into marine sediments buried beneath non-marine sediments dated around the Paleocene-Eocene boundary, to transient uplift. Both Rudge et al. (2008) and Champion et al. (2008) estimated ~ 500 m of uplift that peaked and decayed very quickly over ~ 3 Myr, linking this transient event to the lateral flow of hot material at much

35   shallower mantle depths beneath the lithosphere sourced from a larger mantle anomaly at depth. In comparison, the model maximum transient uplift occurs ~ 4-5 Myr earlier at ~ 60 Ma, and underestimates the total uplift inferred in these studies by half (Fig. 9I). Hartley et al. (2011) reconstructed an ancient drainage network from three-dimensional seismic data in a similar area of the Faroe-Shetland Basin, and subsequently inverted these ancient river profiles to derive a surface uplift

40   history. They proposed that this region was uplifted over three discrete steps of 200-400 m and then

reburied rapidly within ~ 1 Myr around the Paleocene-Eocene boundary (Hartley et al., 2011). A comparison between our model and these results shows, again, a mismatch in the timing of maximum transient uplift of ~4-5 Myr, as our model predicts this to occur earlier at ~ 60 Ma, and a greater mismatch in magnitudes of uplift as our model predicts only 25% of the maximum uplift modelled in

5   Hartley et al. (2011) (Fig. 9J). This mismatch may reflect the higher spatial and temporal resolution of these studies on the mantle-driven effects of the Iceland plume on the evolution of surface topography in the North Atlantic. Our modelling approach does not capture shallow (<350 km depth) mantle or surface processes, which have been suggested to play a significant role in the distribution of the plume-related thermal anomaly. Champion et al. (2008) suggested that the rapid rate of decay of the transient

10   uplift can be linked to the emplacement of the mantle plume at very shallow depths beneath the lithosphere, advected further away by subsequent shallow mantle convective flow. Hartley et al. (2011) proposed that series of hot blobs, sourced from the plume conduit, travelled radially outwards in a horizontal layer in the low-viscosity mantle beneath the lithosphere. They showed that this is geodynamically reasonable in the context of a surface wave tomography model of the upper mantle

15   beneath the region, which images these thermal anomalies maintaining their internal structure up ~ 600 km from the Iceland plume conduit (Delorey et al., 2007), indicating the complexities of upper mantle flow.

In summary, across the Faroe-Shetland and Møre Basins, the model is compatible with the timing and duration of Paleocene anomalous transient uplift that 'interrupts' the subsidence histories in

20   wells located within these basins. The model also predicts dynamic uplift from the late Eocene (~ 40 Ma), associated with the large-scale dynamic effects related to the eastward migration of our model plume toward its present-day location, which is not recorded in the subsidence histories of these basins. The model also predicts plume-related uplift documented along the Norwegian margin during the Paleocene, however, current observations do not constrain the magnitude of uplift.

4.2.5 Explaining anomalous vertical motions along parts of the east and west Greenland margins
Previous efforts focusing on the sedimentary response of the west and east Greenland landscapes to plume-driven uplift used fluvial peneplanation, valley incision, and sediment deposition rates to argue that this uplift was very short lived (< 5 Myr) prior to plume eruption, with the uplift of West

30   Greenland quantified at around several hundred meters, and the East Greenland uplift unable to be quantified (Dam et al., 1998). Apatite fission track data suggest that the present-day high mountains of West Greenland are erosional remnants of continental uplift during the Neogene (Japsen et al., 2005). However, Redfield (2009) argued that the AFT sampling used in this study might be biased. For two locations along the east and west margins of Greenland we compare published water-loaded

35   backstripped tectonic subsidence histories (Clift et al., 1998) against model dynamic topography (Fig. 4, Fig. 9K, 9L). Tectonically, the extensional histories of these margins are temporally offset (Hosseinpour et al, 2013). Along the west Greenland margin continental extension started at ~ 120 Ma (Hosseinpour et al., 2013), with breakup and sea-floor spreading starting in the Labrador Sea at ~ 60 Ma (Oakey and Chalmers, 2012). Along the east Greenland margin, extension started at ~ 80 Ma

40   (Barnett-Moore et al., 2016), and seafloor spreading by ~ 55 Ma (Skogseid et al., 2000). Based on these

extensional histories we expect the slow decay of post-rift subsidence rates to start from continental breakup. For times before ~ 50 Ma, the subsidence histories of Clift et al. (1998) show a near simultaneous timing in the first anomalous transient uplift event starting from ~ 70 Ma and peaking at ~ 60 Ma (Fig. 9K, 9L). Following this, both subsidence histories show an ensuing rate of rapid

5   subsidence and a later secondary anomalous transient uplift episode. Along the east margin of Greenland, at Nugssuaq (Fig. 4), this secondary uplift event is recorded at ~ 53 Ma (Fig. 9L). Along the west Greenland margin at Kangerdlugssuaq (Fig. 4), this secondary transient uplift event occurs slightly earlier at ~ 55 Ma (Fig. 9K). The post-53 Ma tectonic subsidence histories of both basins are unconstrained (Fig. 9K, 9L). The model dynamic topography evolution at these two locations is

10   comparatively different, and reflects the arrival and eastward migration of the model plume through time. At Nugssuaq, the model implies minor dynamic uplift, commencing from 70 Ma. By ~ 65 Ma the largest increase in dynamic uplift of ~ 1000 m is predicted, ending by ~ 60 Ma and entering a continued decline in subsidence (Fig. 9L). This rapid change in significant dynamic uplift reflects the effects of the near-surface arrival of the model plume (Fig. 3). At Kangerdlugssuaq, a similar evolution

15   of dynamic uplift to Nugssuaq is also implied from 60-70 Ma, however, the magnitude of total uplift is less than half of that at Nugssuaq at ~ 400 m (Fig. 9K). This is followed by rapid subsidence until 55 Ma then by two stages of dynamic uplift (Fig. 9K). The first is ~ 30 m in amplitude and lasts until 50 Ma, and the second is ~ 100 m in amplitude and lasts until ~ 40 Ma. For times during the Paleocene and Eocene, these different phases of dynamic uplift and subsidence reflect the eastward migration of

20   the model plume toward and subsequently across the East Greenland margin (Fig. 3).

When comparing the model dynamic topography against these backstripped tectonic histories both locations show agreement on the timing of the first, and largest, transient uplift event culminating at 60 Ma. When comparing magnitudes, the total dynamic uplift from our model at Nugssuaq is ~ 2.5 greater than that estimated from the subsidence history, and the magnitude of uplift is poorly

25   constrained at Kangerdlugssuaq (Fig. 9K). At ~ 55 Ma, at Kangerdlugssuaq, the model dynamic uplift matches this transient event captured in the tectonic subsidence history (Fig. 9K). However, the model suggests uplift occurred over ~ 15 Myr, whereas the limited control points at Kangerdlugssuaq constrain a short-lived uplift event over ~ 1-2 Myr. The model does not capture the second transient uplift event recorded in the tectonic history of the Nugssuaq basin (Fig. 9L).

30   In summary, comparisons at both Kangerdlugssuaq and Nugssuaq show the model is compatible with the timing of maximum transient uplift at 60 Ma associated with the arrival of the model plume. Yet, the model overpredicts the magnitude of total uplift at both locations and does not account for a secondary transient uplift event at ~ 55 Ma. Along the East Greenland margin, the more frequent Cenozoic changes between model dynamic uplift and subsidence reflect the progressive

35   eastward motion of the model plume beneath Greenland.

4.3. Mismatches between the timing, amplitude, and spatial evolution of the model dynamic topography and observational constraints

Comparing the model dynamic topography to available published geological and geophysical

40   observations (Fig. 6-9) highlights mismatches in the spatial, temporal, and amplitude evolutions

(section 4.2). Temporal mismatches are at most 10 Myr across the North Atlantic (section 4.2). Generally, maximum uplift associated with the near-surface arrival of the Iceland plume, is observed to occur sometime in the Paleocene and early Eocene between ~60-50 Ma (section 4.2; Fig. 6-9), as the model predicts maximum uplift at ~ 60 Ma across the region (Fig. 6-9). Since the model temporal

5   resolution is ~ 5 Myr (section 2), this mismatch of up to ~ 10 Myr in the timing of maximum uplift is not unexpected.

A qualitative comparison between the model dynamic topography and the mapped time-dependent trail of extrusive magmatic rocks constraining the approximate spatial evolution of the plume beneath the North Atlantic suggests the model plume motion path can be considered sensible (Fig. 3). Together

10   with previous geological models (section 4.1), this supports the near-surface arrival of the Iceland plume somewhere beneath the West Greenland margin (Clift et al., 1998), and its subsequent southeastward motion until present-day. The long-wavelength nature of the model dynamic topography results in the gradual dynamic uplift of the northwest European margin since the mid Eocene (~ 35 Ma onwards) related to the continued eastward migration of the model plume (Fig. 4-9). This produces a

15   mismatch between the subsidence histories of the Porcupine, Rockall, Faroe-Shetland, Møre, and North Sea Basins (except for well 15-17-9) and the model dynamic topography evolution, as these basins do not preserve evidence of continual dynamic uplift from the Eocene until present-day (Fig. 6-9). However, we suggest that the gradual increase in dynamic uplift since this time could potentially contribute to the current debate surrounding the explanation of observed anomalous Eocene uplift as

20   reviewed in Anell et al. (2009) or younger anomalous uplift in the Neogene (Praeg et al., 2005) across the northeast Atlantic Ocean.

A qualitative comparison between the evolution of dynamic topography amplitudes, and the magnitude of preserved anomalous subsidence shows the modelled plume-related uplift is underestimated by as much as several hundred meters in some parts of the North Atlantic (e.g. Faroe-

25   Shetland Basin; section 4.2.4). The amplitude of predicted dynamic topography depends on the adopted definition of dynamic topography (see Flament et al., 2013) and boundary conditions for the calculation (e.g. Thoraval and Richards, 1997). Here, we compute water-loaded surface dynamic topography from buoyancy sources deeper than 350 km and with free-slip boundary conditions. Including shallower buoyancy sources and using no-slip boundary conditions (e.g. Flament et al., 2014)

30   would increase the amplitude of predicted dynamic topography. In addition, the mantle flow models used here do not account for the complex evolution of shallow (<350 km) asthenospheric flow, or the complex interplay between mantle, lithosphere, and surface processes, which are known to have played an important role in the evolution of the major basins in the North Atlantic during the Cenozoic (e.g. Nielsen et al., 2002).

35   In summary, this comparison shows our new dynamic topography model predicts a reasonable spatial and temporal evolution of the Iceland plume, which accounts for contemporaneous Paleocene vertical motions across the North Atlantic. The main mismatch concerns the underestimation of maximum uplift magnitudes during the Paleocene, and possibly the onset in the continuous dynamic uplift in the northeast Atlantic from the mid-Eocene.

5. Conclusion

Analysing the deep lower mantle flow predicted by a 3D model indicates that over the last ~ 100 Myr a consistent pattern of convergent flow persists in the lowermost mantle near the tip of the African LLSVP, which remains remarkably stable over this period, making it an ideal plume nucleation site.

5   The arrival location of the rotated model plume is in reasonable agreement with previous geological models that support its near surface arrival somewhere beneath western Greenland during the Paleocene. The motion path of the rotated model plume is in agreement with the regional volcanic record. A comparison between model dynamic topography and published constraints shows that widespread Paleocene and early Eocene uplift across the region can be explained by the mantle-driven

10   effects of a large plume ~ 2000 km in diameter, first arriving beneath central western Greenland. In some parts of the North Atlantic the mantle flow model underestimates the magnitude of observed anomalous surface vertical motions during the Paleocene by several hundred meters. We attribute this mismatch in magnitudes to the additional effects of shorter wavelength upper mantle flow and surface processes, not captured in our modelling approach.

6. Acknowledgements

This research was undertaken with the assistance of resources from the National Computational Infrastructure (NCI), which is supported by the Australian Government. The authors were supported by Australian Research Council grants IH130200012 and DP130101946. Figures were constructed using

20   the Generic Mapping Tools and Python libraries (Fig. 1 only).

25   **8. References**

Anell, I., Thybo, H., and Artemieva, I., 2009, Cenozoic uplift and subsidence in the North Atlantic region: geological evidence revisited: Tectonophysics, v. 474, no. 1, p. 78-105.

Artemieva, I. M., 2006, Global 1× 1 thermal model TC1 for the continental lithosphere: implications for lithosphere secular evolution: Tectonophysics, v. 416, no. 1, p. 245-277.

30   Auer, L., Boschi, L., Becker, T., Nissen-Meyer, T. & Giardini, D. *Savani*: a variable resolution whole-mantle model of anisotropic shear velocity variations based on multiple data sets. *J. Geophys. Res.* **119,** 3006–3034 (2014).

Barnett-Moore, N., Flament, N., Heine, C., Butterworth, N., and Müller, R. D., 2014, Cenozoic uplift of south Western Australia as constrained by river profiles: Tectonophysics, v. 622, p. 186-197.

35   Barnett-Moore, N., Müller, R. D., Williams, S., Skogseid, J., and Seton, M., 2016, A reconstruction of the North Atlantic since the earliest Jurassic: Basin Research, v. In Review.

Bertram, G., and Milton, N., 1988, Reconstructing basin evolution from sedimentary thickness; the importance of palaeobathymetric control, with reference to the North Sea: Basin Research, v. 1, no. 4, p. 247-257.

Bower, D. J., Gurnis, M., and Seton, M., 2013, Lower mantle structure from paleogeographically constrained dynamic Earth models: Geochemistry, Geophysics, Geosystems, v. 14, no. 1, p. 44-63.

Bower, D. J., Gurnis, M., and Flament, N, 2015, Assimilating lithosphere and slab history in 4-D Earth models, *Physics of the Earth and Planetary Interiors*, 238, 8-22.

Boyden, J. A., Müller, R. D., Gurnis, M., Torsvik, T. H., Clark, J. A., Turner, M., Ivey-Law, H., Watson, R. J., and Cannon, J. S., 2011, Next-generation plate-tectonic reconstructions using GPlates: Geoinformatics: cyberinfrastructure for the solid earth sciences, p. 95-114.

Chalmers, J., Larsen, L., and Pedersen, A., 1995, Widespread Palaeocene volcanism around the northern North Atlantic and Labrador Sea: evidence for a large, hot, early plume head: Journal of the Geological Society, v. 152, no. 6, p. 965-969.

Champion, M., White, N., Jones, S., and Lovell, J., 2008, Quantifying transient mantle convective uplift: An example from the Faroe‐Shetland basin: Tectonics, v. 27, no. 1.

Christensen, U. R, and Yuen, D., A., 1985, Layered convection induced by phase transitions, *Journal of Geophysical Research: Solid Earth*, 90, 10291-10300.

Clift, P., 1996, Plume tectonics as a cause of mass wasting on the southeast Greenland continental margin: Marine and Petroleum Geology, v. 13, no. 7, p. 771-780.

Clift, P. D., and Turner, J., 1995, Dynamic support by the Icelandic plume and vertical tectonics of the northeast Atlantic continental margins: Journal of Geophysical Research: Solid Earth, v. 100, no. B12, p. 24473-24486.

-, 1998, Paleogene igneous underplating and subsidence anomalies in the Rockall-Faeroe-Shetland area: Marine and Petroleum Geology, v. 15, no. 3, p. 223-243.

Dam, G., Larsen, M., and Sønderholm, M., 1998, Sedimentary response to mantle plumes: implications from Paleocene onshore successions, West and East Greenland: Geology, v. 26, no. 3, p. 207-210.

Delorey, A. A., Dunn, R. A., and Gaherty, J. B., 2007, Surface wave tomography of the upper mantle beneath the Reykjanes Ridge with implications for ridge-hot spot interaction: Journal of Geophysical Research, v. 112, no. B08313.

Doubrovine, P. V., Steinberger, B., and Torsvik, T. H., 2012, Absolute plate motions in a reference frame defined by moving hot spots in the Pacific, Atlantic, and Indian oceans: Journal of Geophysical Research: Solid Earth, v. 117, no. B9.

-, 2016, A failure to reject: Testing the correlation between large igneous provinces and deep mantle structures with EDF statistics: Geochemistry, Geophysics, Geosystems, v. 17, no. 3, p. 1130-1163.

Erratt, D., Thomas, G., and Wall, G., The evolution of the central North Sea Rift, *in* Proceedings Geological Society, London, Petroleum Geology Conference series1999, Volume 5, Geological Society of London, p. 63-82.

Fahnestock, M., Abdalati, W., Joughin, I., Brozena, J., and Gogineni, P., 2001, High geothermal heat flow, basal melt, and the origin of rapid ice flow in central Greenland: Science, v. 294, no. 5550, p. 2338-2342.

Flament, N., Gurnis, M., Williams, S. E., Seton, M., Skogseid, J., Heine, C., and Müller, R. D., 2014, Topographic asymmetry of the South Atlantic from global models of mantle flow and lithospheric stretching: Earth and Planetary Science Letters.

Flament, N., Gurnis, M., and Müller, R. D., 2013, A review of observations and models of dynamic topography: Lithosphere, v. 5, no. 2, p. 189-210.

Fletcher, R., Kusznir, N., Roberts, A., and Hunsdale, R., 2013, The formation of a failed continental breakup basin: The Cenozoic development of the Faroe‐Shetland Basin: Basin Research, v. 25, no. 5, p. 532-553.

Green, P. F., 2002, Early Tertiary paleo-thermal effects in Northern England: reconciling results from apatite fission track analysis with geological evidence: Tectonophysics, v. 349, no. 1, p. 131-144.

Hartley, R. A., Roberts, G. G., White, N., and Richardson, C., 2011, Transient convective uplift of an ancient buried landscape: Nature Geoscience, v. 4, no. 8, p. 562-565.

Hassan, R., Flament, N., Gurnis, M., Bower, D. J., and Müller, D., 2015, Provenance of plumes in global convection models: Geochemistry, Geophysics, Geosystems, v. 16, no. 5, p. 1465-1489.

Hosseinpour, M., Müller, R., Williams, S., and Whittaker, J., 2013, Full-fit reconstruction of the Labrador Sea and Baffin Bay: Solid Earth, v. 4, p. 461-479.

Huuse, M., 2002, Cenozoic uplift and denudation of southern Norway: insights from the North Sea Basin: Geological Society, London, Special Publications, v. 196, no. 1, p. 209-233.

Ismail-Zadeh, A., Korotkii, A., Schubert, G., and Tsepelev, I., 2009, Numerical techniques for solving the inverse retrospective problem of thermal evolution of the Earth interior: Computers & Structures, v. 87, no. 11, p. 802-811.

Japsen, P., Green, P. F., and Chalmers, J. A., 2005, Separation of Palaeogene and Neogene uplift on Nuussuaq, West Greenland: Journal of the Geological Society, v. 162, no. 2, p. 299-314.

Jarvis, G. T., and McKenzie, D. P., 1980, Sedimentary basin formation with finite extension rates: Earth and Planetary Science Letters, v. 48, no. 1, p. 42-52.

Jones, S. M., White, N., and Lovell, B., 2001, Cenozoic and Cretaceous transient uplift in the Porcupine Basin and its relationship to a mantle plume: Geological Society, London, Special Publications, v. 188, no. 1, p. 345-360.

Joy, A. M., 1992, Right place, wrong time: anomalous post-rift subsidence in sedimentary basins around the North Atlantic Ocean: Geological Society, London, Special Publications, v. 68, no. 1, p. 387-393.

Kaban, M. K., Petrunin, A. G., Schmeling, H., and Shahraki, M., 2014, Effect of decoupling of lithospheric plates on the observed geoid: Surveys in Geophysics, v. 35, no. 6, p. 1361-1373.

Karato, S., and Wu., P. 1993, Rheology of the upper mantle - A synthesis, *Science*, 260, 771-778.

Lekic, V., Cottaar, S., Dziewonski, A. & Romanowicz, B. Cluster analysis of global lower mantle tomography: a new class of structure and implications for chemical heterogeneity. *Earth Planet. Sci. Lett.* **357/358,** 68–77 (2012).

Lewis, C. L., Green, P. F., Carter, A., and Hurford, A. J., 1992, Elevated K/T palaeotemperatures throughout Nortwest England: three kilometres of Tertiary erosion?: Earth and Planetary Science Letters, v. 112, no. 1, p. 131-145.

Milton, N., Bertram, G., and Vann, I., 1990, Early Palaeogene tectonics and sedimentation in the Central North Sea: Geological Society, London, Special Publications, v. 55, no. 1, p. 339-351.

Morgan, W. J., 1971, Convection plumes in the lower mantle.

Mudge, D. C., and Jones, S. M., 2004, Palaeocene uplift and subsidence events in the Scotland–Shetland and North Sea region and their relationship to the Iceland Plume: Journal of the Geological Society, v. 161, no. 3, p. 381-386.

Müller, R. D., Royer, J.-Y., and Lawver, L. A., 1993, Revised plate motions relative to the hotspots from combined Atlantic and Indian Ocean hotspot tracks: Geology, v. 21, no. 3, p. 275-278.

Nielsen, S., Paulsen, G., Hansen, D., Gemmer, L., Clausen, O., Jacobsen, B., Balling, N., Huuse, M., and Gallagher, K., 2002, Paleocene initiation of Cenozoic uplift in Norway: Geological Society, London, Special Publications, v. 196, no. 1, p. 45-65.

Noble, R., Macintyre, R., and Brown, P., 1988, Age constraints on Atlantic evolution: timing of magmatic activity along the E Greenland continental margin: Geological Society, London, Special Publications, v. 39, no. 1, p. 201-214.

O'Neill, C., Müller, D., and Steinberger, B., 2005, On the uncertainties in hot spot reconstructions and the significance of moving hot spot reference frames: Geochemistry, Geophysics, Geosystems, v. 6, no. 4.

Oakey, G. N., and Chalmers, J. A., 2012, A new model for the Paleogene motion of Greenland relative to North America: plate reconstructions of the Davis Strait and Nares Strait regions between Canada and Greenland: Journal of Geophysical Research: Solid Earth (1978–2012), v. 117, no. B10.

Parnell-Turner, R., White, N., Henstock, T., Murton, B., Maclennan, J., and Jones, S. M., 2014, A continuous 55-million-year record of transient mantle plume activity beneath Iceland: Nature Geoscience, v. 7, no. 12, p. 914-919.

Peron-Pinvidic, G., Manatschal, G., and Osmundsen, P. T., 2013, Structural comparison of archetypal Atlantic rifted margins: a review of observations and concepts: Marine and Petroleum Geology, v. 43, p. 21-47.

Planke, S., Skogseid, J., and Eldholm, O., 1991, Crustal structure off Norway, 62 to 70 north: Tectonophysics, v. 189, no. 1, p. 91-107.

Praeg, D., Stoker, M., Shannon, P., Ceramicola, S., Hjelstuen, B., Laberg, J., and Mathiesen, A., 2005, Episodic Cenozoic tectonism and the development of the NW European 'passive' continental margin: Marine and Petroleum Geology, v. 22, no. 9, p. 1007-1030.

Redfield, T., 2010, On apatite fission track dating and the Tertiary evolution of West Greenland topography: Journal of the Geological Society, v. 167, no. 2, p. 261-271.

Ren, S., Faleide, J. I., Eldholm, O., Skogseid, J., and Gradstein, F., 2003, Late Cretaceous–Paleocene tectonic development of the NW Vøring basin: Marine and Petroleum Geology, v. 20, no. 2, p. 177-206.

Rickers, F., Fichtner, A., and Trampert, J., 2013, The Iceland–Jan Mayen plume system and its impact on mantle dynamics in the North Atlantic region: evidence from full-waveform inversion: Earth and Planetary Science Letters, v. 367, p. 39-51.

Roberts, A. M., Corfield, R. I., Kusznir, N. J., Matthews, S. J., Hansen, E.-K., and Hooper, R. J., 2009, Mapping palaeostructure and palaeobathymetry along the Norwegian Atlantic continental margin: Møre and Vøring basins: Petroleum Geoscience, v. 15, no. 1, p. 27-43.

Roberts, A. M., Lundin, E. R., and Kusznir, N. J., 1997, Subsidence of the Vøring Basin and the influence of the Atlantic continental margin: Journal of the Geological Society, v. 154, no. 3, p. 551-557.

Rogozhina, I., Petrunin, A. G., Vaughan, A. P., Steinberger, B., Johnson, J. V., Kaban, M. K., Calov, R., Rickers, F., Thomas, M., and Koulakov, I., 2016, Melting at the base of the Greenland ice sheet explained by Iceland hotspot history: Nature Geoscience.

Saunders, A., Fitton, J., Kerr, A. C., Norry, M., and Kent, R., 1997, The north Atlantic igneous province: Large igneous provinces: Continental, oceanic, and planetary flood volcanism, p. 45-93.

Saunders, A. D., Larsen, H. C., and Fitton, J. G., 1998, Magmatic development of the southeast Greenland margin and evolution of the Iceland Plume: Geochemcial constraints from IODP Leg 1521.

Rudge, J. F., Champion, M. E. S., White, N., McKenzie, D., and Lovell, B., 2008, A plume model of transient diachronous uplift at the Earth's surface: Earth and Planetary Science Letters, v. 267, no. 1, p. 146-160.

Skogseid, J., Planke, S., Faleide, J. I., Pedersen, T., Eldholm, O., and Neverdal, F., 2000, NE Atlantic continental rifting and volcanic margin formation: Special Publication – Geological Society of London, v. 167, p. 295-326.

Smallwood, J., and White, R., 2002, Ridge-plume interaction in the North Atlantic and its influence on continental breakup and seafloor spreading: Geological Society, London, Special Publications, v. 197, no. 1, p. 15-37.

Smallwood, J. R., and Gill, C. E., 2002, The rise and fall of the Faroe–Shetland Basin: evidence from seismic mapping of the Balder Formation: Journal of the Geological Society, v. 159, no. 6, p. 627-630.

Spice, H. E., Fitton, J. G., and Kirstein, L. A., 2016, Temperature fluctuation of the Iceland mantle plume through time: Geochemistry, Geophysics, Geosystems.

Steinberger, B., Spakman, W., Japsen, P., and Torsvik, T. H., 2014, The key role of global solid‐Earth processes in preconditioning Greenland's glaciation since the Pliocene: Terra Nova, v. 27, no. 1, p. 1-8.

Steinberger, B., and Calderwood A., R., 2006, Models of large-scale viscous flow in the Earth's mantle with constraints from mineral physics and surface observations, *Geophysical Journal International*, 167, 1461-1481.

Steinberger, B., Sutherland, R., and O'connell, R. J., 2004, Prediction of Emperor-Hawaii seamount locations from a revised model of global plate motion and mantle flow: Nature, v. 430, no. 6996, p. 167-173.

Stoker, M., 1997, Mid-to late Cenozoic sedimentation on the continental margin off NW Britain: Journal of the Geological Society, v. 154, no. 3, p. 509-515.

Storey, M., Duncan, R. A., and Tegner, C., 2007, Timing and duration of volcanism in the North Atlantic Igneous Province: Implications for geodynamics and links to the Iceland hotspot: Chemical Geology, v. 241, no. 3, p. 264-281.

Stuart, F. M., Lass-Evans, S., Fitton, J. G., and Ellam, R. M., 2003, High 3He/4He ratios in picritic basalts from Baffin Island and the role of a mixed reservoir in mantle plumes: Nature, v. 424, no. 6944, p. 57-59.

Tackley, P. J., 1996, Effects of strongly variable viscosity on three dimensional compressible convection in planetary mantles, *Journal of Geophysical Research: Solid Earth*, 101, 3311-3332.

Tate, M., White, N., and Conroy, J. J., 1993, Lithospheric extension and magmatism in the Porcupine Basin west of Ireland: Journal of Geophysical Research: Solid Earth (1978–2012), v. 98, no. B8, p. 13905-13923.

Tegner, C., Brooks, C., Duncan, R., Heister, L., and Bernstein, S., 2008, 40 Ar–39 Ar ages of intrusions in East Greenland: Rift-to-drift transition over the Iceland hotspot: Lithos, v. 101, no. 3, p. 480-500.

Torsvik, T. H., Amundsen, H. E., Trønnes, R. G., Doubrovine, P. V., Gaina, C., Kusznir, N. J., Steinberger, B., Corfu, F., Ashwal, L. D., and Griffin, W. L., 2015, Continental crust beneath southeast Iceland: Proceedings of the National Academy of Sciences, v. 112, no. 15, p. E1818-E1827.

Torsvik, T. H., Mosar, J., and Eide, E. A., 2001, Cretaceous–tertiary geodynamics: a North Atlantic exercise: Geophysical Journal International, v. 146, no. 3, p. 850-866.

Tosi, N., Yuen D. A., De Koker N., and Wentzcovitch R. M., 2013, Mantle dynamics with pressure- and temperature-dependent thermal expansivity and conductivity, *Physics of the Earth and Planetary Interiors*, 217, 48-58.

Thoraval, C., and Richards, M. A., 1997, The geoid constraint in global geodynamics: viscosity structure, mantle heterogeneity models and boundary conditions: Geophysical Journal International, v. 131, no. 1, p. 1-8.

Upton, B., Emeleus, C., Rex, D., and Thirlwall, M., 1995, Early tertiary magmatism in NE Greenland: Journal of the Geological Society, v. 152, no. 6, p. 959-964.

Wessel, P., Smith, W. H., Scharroo, R., Luis, J., and Wobbe, F., 2013, Generic Mapping Tools: Improved Version Released: Eos, Transactions American Geophysical Union, v. 94, no. 45, p. 409-410.

White, R., Bown, J., and Smallwood, J., 1995, The temperature of the Iceland plume and origin of outward-propagating V-shaped ridges: Journal of the Geological Society, v. 152, no. 6, p. 1039-1045.

White, R., and McKenzie, D., 1989, Magmatism at rift zones: the generation of volcanic continental margins and flood basalts: Journal of Geophysical Research: Solid Earth (1978–2012), v. 94, no. B6, p. 7685-7729.

Zhong, S., Mcnamara A., Tan E., Moresi L., Gurnis M., 2008, A benchmark study on mantle convection in a 3D spherical shell using CitcomS, *Geochemistry, Geophysics, Geosystems*, 9.

Parameter	Symbol	Value	Units
Rayleigh number	Ra	5×10^8	-
Earth radius	R_0	6371	km
Density	ρ_0	3930	$Kg\ m^{-3}$
Thermal expansivity	α_0	1.42×10^{-5}	K^{-1}
Thermal diffusivity	κ_0	1×10^{-6}	$m^2\ s^{-1}$
Specific heat capacity	C_p	1100	$Jkg^{-1}\ K^{-1}$
Gravitational acceleration	g	10	ms^{-2}
Surface Temperature	T_s	300	K
Dissipation number	Di	0.8	-
Reference Viscosity	η_0	1×10^{21}	Pa S
Internal Heating	H	100	-

Table 1: Model parameters.
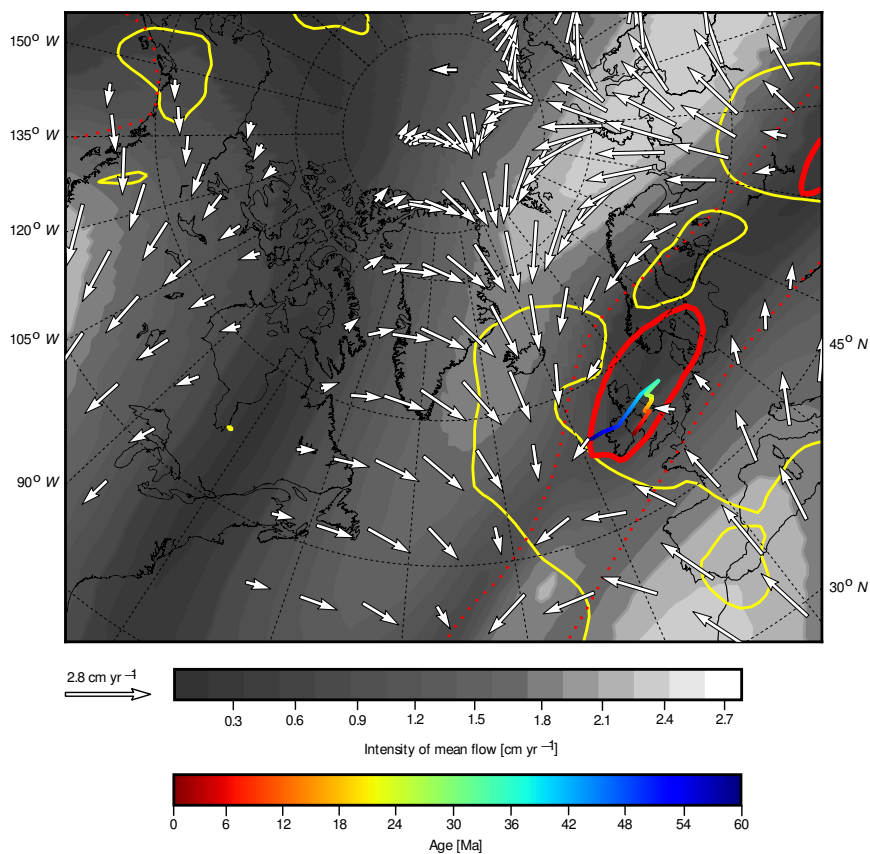
Figure 1: **The magnitude of mean flow velocity in a 300 km thick shell above the CMB, time-averaged over the last 100 Ma is shown in grey shading and associated flow directions are shown by white arrows. Flow directions are not shown for regions where flow magnitudes are smaller than their standard deviation, σ, to avoid visual clutter. The 75% chemical concentration**

5 **isosurface of the dense chemical layer above the CMB, time-averaged over the last 100 Ma, defines the mean location of model LLSVPs over the period. The dotted red contour shows the mean location of the edges of the northern tip of model African LLSVP, 200 km above the CMB. The solid red contour shows the same, but at 320 km above the CMB. The yellow contour shows the 0.5% slow contour of the SAVANI tomography model (Auer et al. 2014) at 50 km above the**

10 **CMB. The multi-coloured trajectory shows the motion of the model Iceland plume – in the mantle frame of reference – since its arrival near the surface at 60 Ma. The thin black dotted arrow denotes the distance between the model and inferred present-day plume location.**
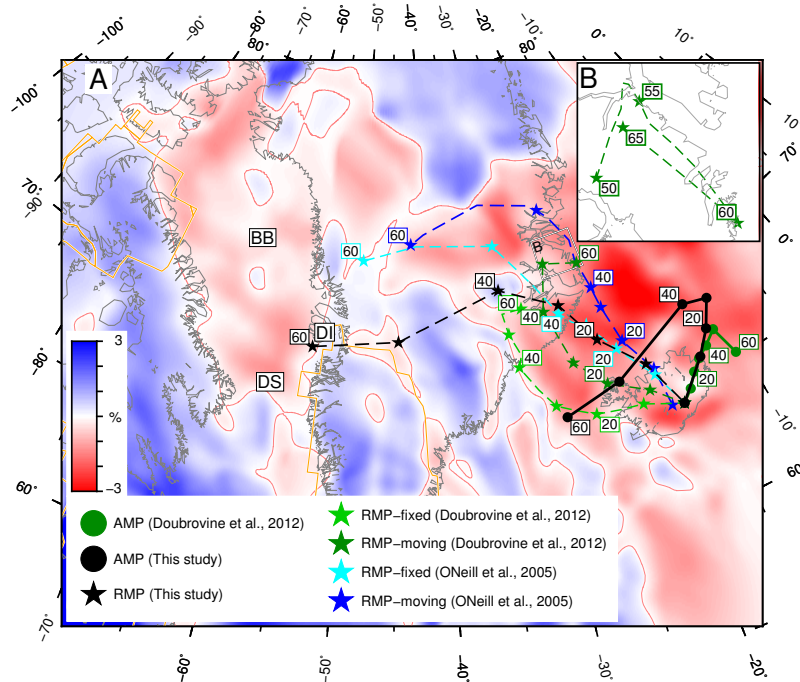
Figure 2: **(A) Reconstructed absolute motion paths of the Iceland plume (solid bold circles) and its reconstructed relative motion paths to Greenland (solid smaller stars). Black: model motion paths (section 2.2.3) after its surface rotation (section 3.2); Green: motion paths of Doubrovine et al. (2012); Blue: motion paths of O'Neill et al. (2005). Underlain is the 150 km depth slice of a P-**

20 **wave velocity model (Jakovlev et al., 2012) presented in Rogozhina et al. (2016), showing the**

velocity model beneath Baffin Bay and Davis Straight and Greenland, colour-mapped for percentage velocity anomaly. (B) Relative motion path of the reconstructed moving hotspot track of Iceland relative to Greenland between 65 and 50 Ma inferred by Doubrovine et al. (2012). DI: Disko Island; BB: Baffin Bay; DS: Davis Straight.
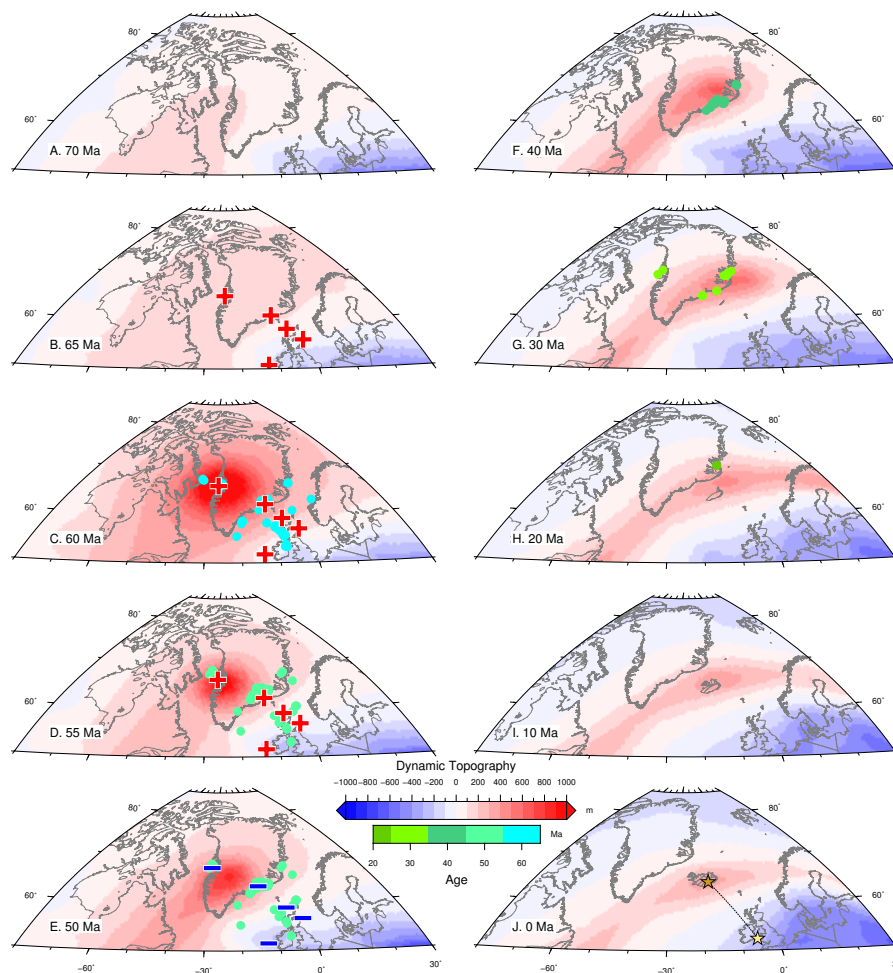
Figure 3: (A-J) Predicted Cenozoic North Atlantic dynamic topography in the mantle frame of reference, after rotation of the results based on the present-day location of the mantle plume. Circles colour-coded by age represent a compiled set of extrusive volcanics related to plume activities across the North Atlantic (Spice et al., 2016; Torsvik et al., 2001) in 10 Myr intervals (± 5 Myr for each reconstructed time) and reconstructed in the mantle frame of reference. Positive (red crosses) and negative (blue dashes) signs correspond to the timings in transient uplift and subsequent subsidence, respectively, based on published observations compiled in Figs 5-9. Light

gold star in J shows the present-day location of the model plume, dark gold star shows the present-day location of the plume based on Torsvik et al. (2015), and the thin black line illustrates the rotation applied to the model.
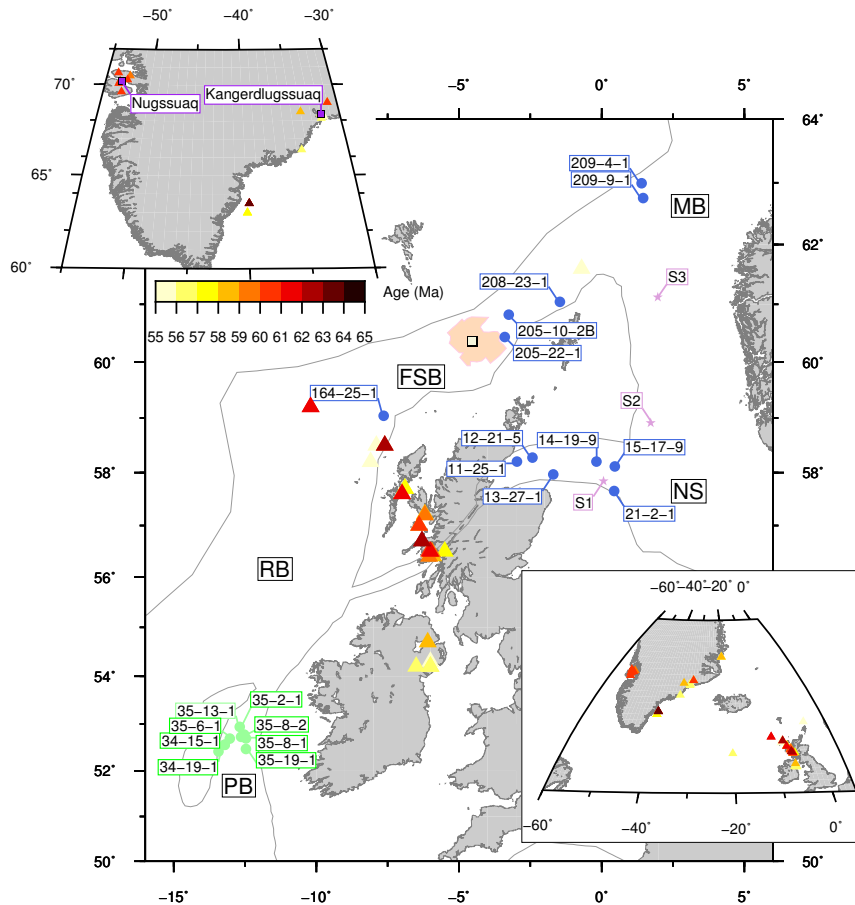
Figure 4: Map view locations of the compiled dataset used to compare against the evolution of model dynamic topography. Solid blue circles: locations of wells that were backstripped for their water-loaded tectonic subsidence histories in Clift and Turner (1998); solid green circles: locations of wells that were backstripped for their water-loaded tectonic subsidence histories in

10 **Jones et al. (2001); solid pink stars are locations of modelled stratigraphic cross sections from Nadin et al. (1997); solid beige region represents area of 3D seismic data coverage used in the analytical modelling approaches of Hartley et al. (2012) and Champion et al. (2008). Coloured triangles are age-coded plume-related extrusive volcanics from 55-65 Ma only (taken from the compilation of Torsvik et al., 2001). MB: Møre Basin; FSB: Faroe-Shetland Basin; RB: Rockall**

Basin; PB: Porcupine Basin; NS: North Sea. Lower inset shows an overview of the northeast Atlantic region and the distribution of age-coded plume-related extrusive volcanics. Upper inset shows two additional locations (purple squares) on the east and west Greenland margins where backstripped water-loaded tectonic subsidence histories were derived in Clift et al. (1998).
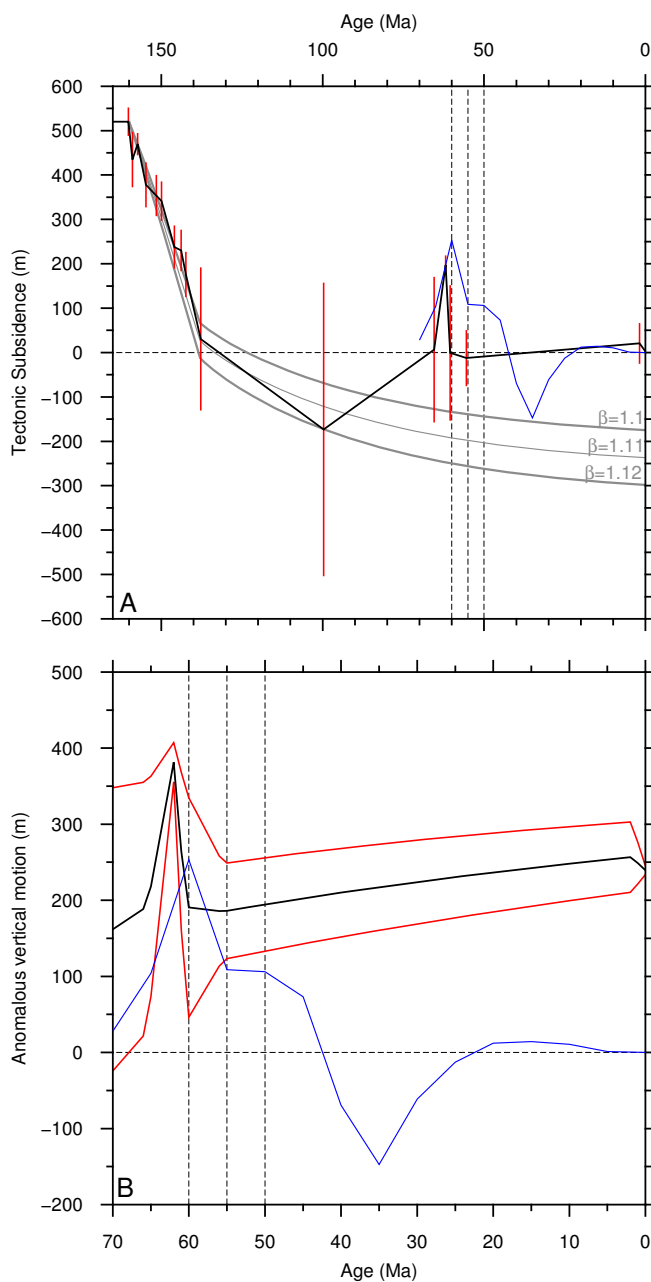
Figure 5: (A) An example of comparing a backstripped water-loaded tectonic subsidence history (solid black curve; Clift and Turner, 1998) against several corresponding modelled water-loaded tectonic subsidence histories (light grey curves; Jarvis and McKenzie, 1980) from well 13-27-1 in

the North Sea. Deviations between these curves can be interpreted as anomalous subsidence inconsistent with expected post-rift thermal subsidence (Jarvis and McKenzie, 1980). Red bars represent errors in subsidence magnitudes related to uncertainties in palaeobathymetry depth estimates (Clift and Turner, 1998). The solid blue curve is the model dynamic topography at this well location (Fig. 3) (section 2.2.3; Fig. 3). The three vertical light grey dotted lines represent ages 50, 55, and 60 Ma; the horizontal grey dotted line is zero elevation. (B) Anomalous vertical motion (thick black curve) calculated by subtracting the best fit modelled tectonic subsidence history (β = 1.11) away from the subsidence history in (A), focused on the last 70 Myr. Red curves represent errors in anomalous subsidence estimates related to the uncertainty in palaeobathymetry depth mentioned in (A). Thin grey dotted lines and blue curve same as in (A).
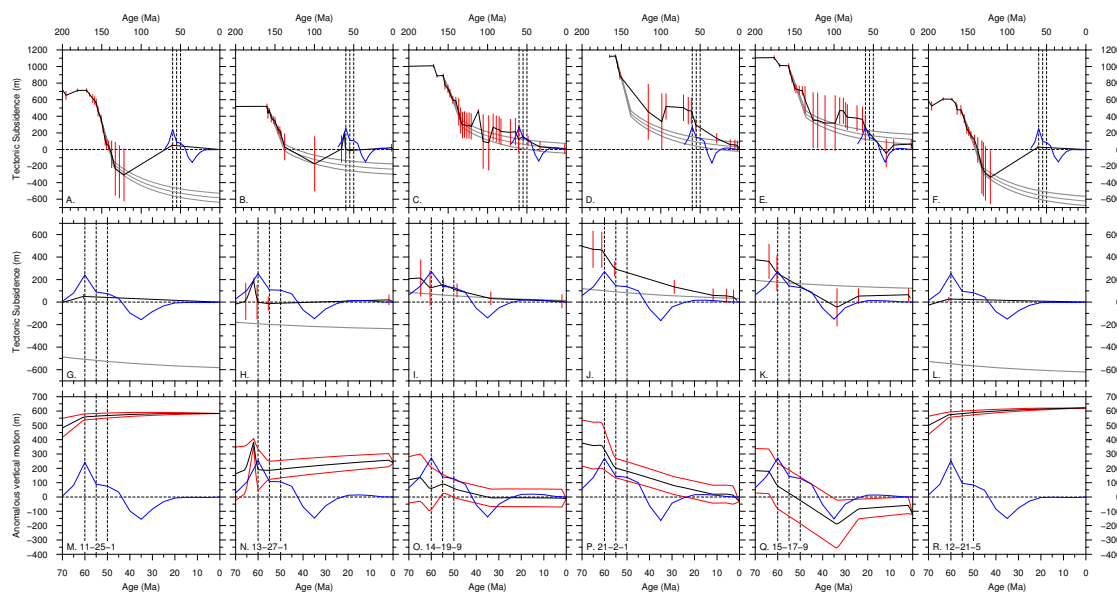
Figure 6: Top panels (A-F): Backstripped water-loaded tectonic subsidence histories from wells in the North Sea (locations given in Fig. 4; Clift and Turner, 1998), presented as in Fig. 5A Middle panels (G-L): Focus on the last 70 Myr of top panels. Bottom panels (M-R): Comparison between model dynamic topography and anomalous vertical motion curves presented as in Fig. 5B. .
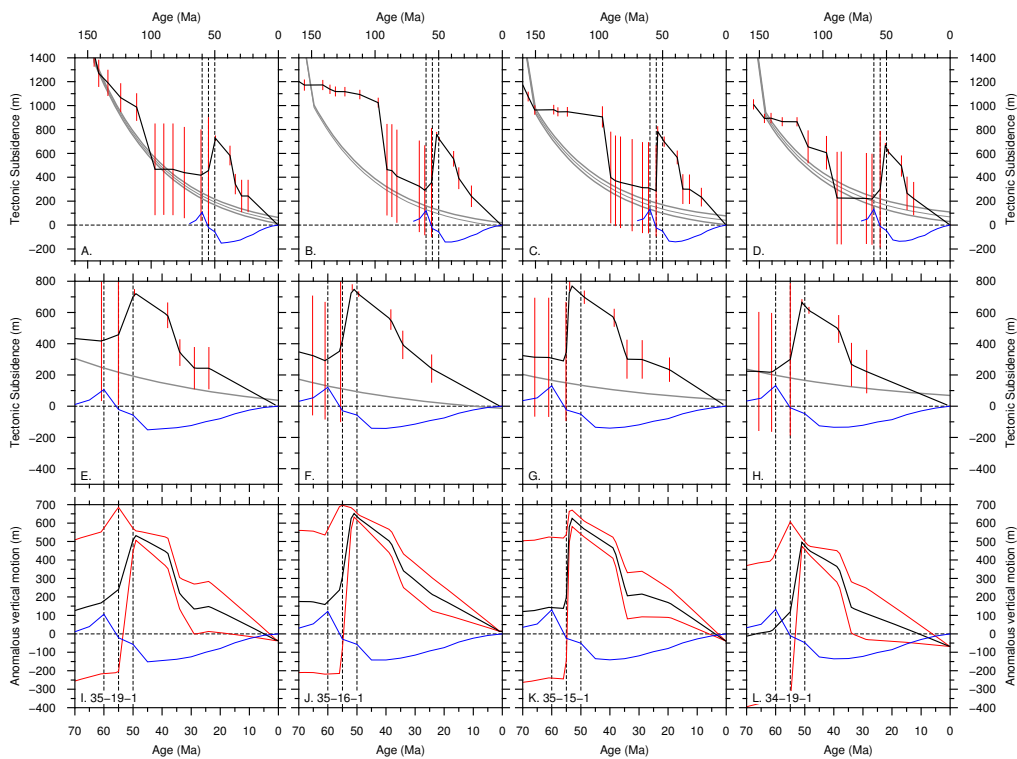
5   **Figure 7: Same as Fig. 6 except for wells reproduced from Jones et al. (2001) in the Porcupine Basin (locations given in Fig. 4).**
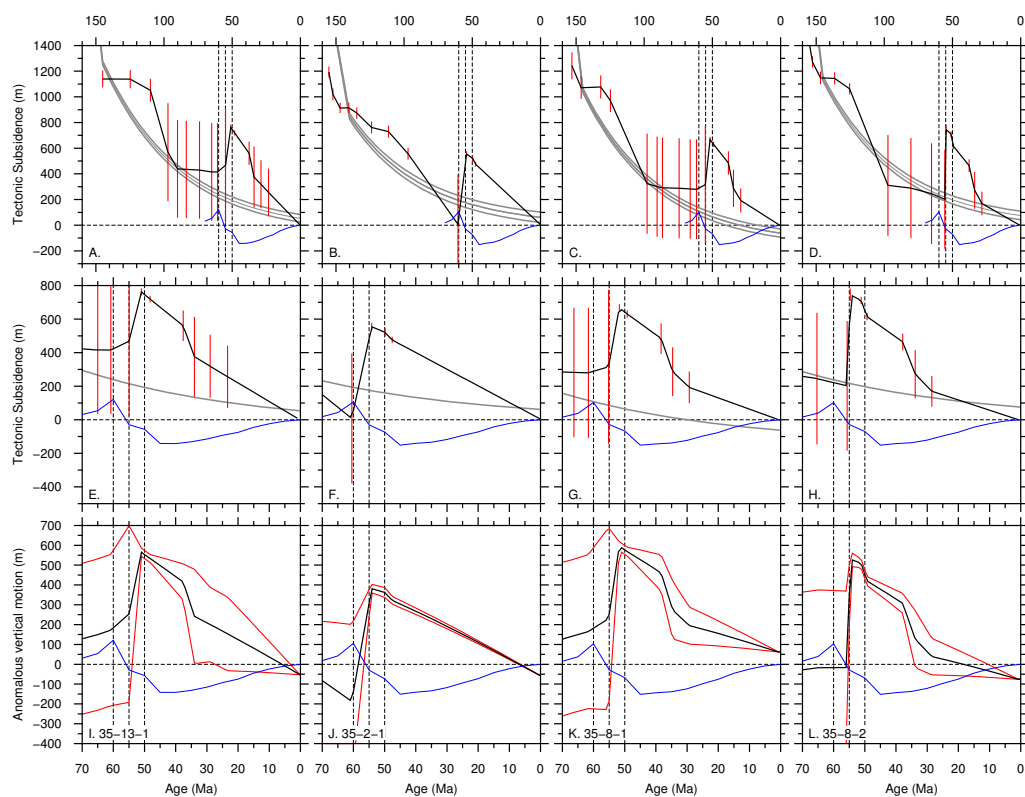
Figure 8: Same as Fig. 7 for wells reproduced from Jones et al. (2001) in the Porcupine Basin (locations given in Fig. 4).
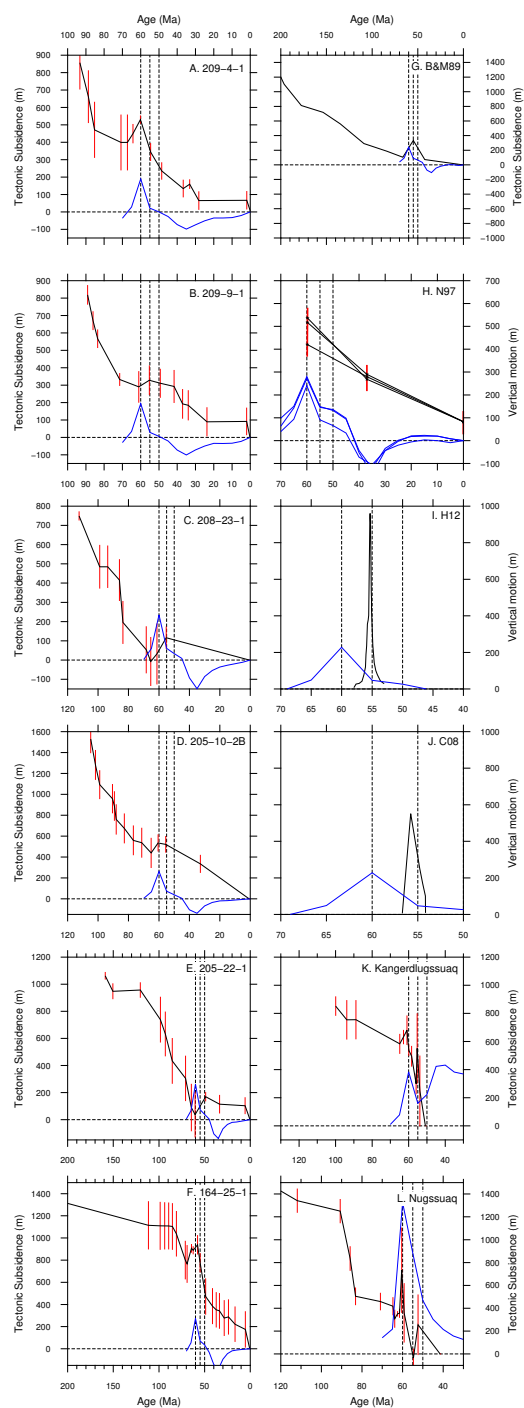
Figure 9: (A-F) Backstripped water-loaded tectonic subsidence histories for two wells in the southern Møre Basin (A-B; locations given in Fig. 4; Clift and Turner, 1998), and Faroe-Shetland Basin (C-F; locations given in Fig. 4; Clift and Turner, 1998). (G) Water-loaded tectonic

5 **subsidence history reproduced from Bertram and Milton (1989), published without palaeobathymetry error bars. (H) Evolution of decaying uplift calculated from modelled stratigraphic sections across the North Sea reproduced from Nadin et al. (1997). Given the long wavelength nature of the model dynamic topography, and the relatively close proximity of the three stratigraphic sections (Fig. 4; stars) we include all three results in this plot. Red error bars**

10 **represent uncertainty in uplift decay over time. The blue curve on each plot is the corresponding time-dependent evolution of dynamic topography (section 2.2.3) for each site (Fig. 4). (I) Modelled uplift history from Hartley et al. (2012) – see main text for description.(J) Modelled uplift history from Champion et al. (2008) – see main text for description. (K-L) backstripped water-loaded tectonic subsidence histories for two locations on the east and west Greenland**

15 **margins (Fig. 3) from Clift et al. (1998). Blue dynamic topography curve through time derived as described in Fig. 5.**